X-ray, extreme and far ultraviolet optical thin films for space applications

Muamer Zukic, Douglas G. Torr and Jongmin Kim

University of Alabama in Huntsville
Physics Department
Optics Building 300
Huntsville, AL 35899
U. S. A.
Phone: (205) 895-6238 ext. 374
Fax: (205) 895-6717

1.0 INTRODUCTION

Far and extreme ultraviolet (FUV: 120-200 nm, EUV: 30-120 nm) optical thin film filters find many uses in space astronomy, space astrophysics, and space aeronomy. Spacebased spectrographs are used for studying emission and absorption features of the earth, planets, sun, stars, and the interstellar medium. Most of these spectrographs use transmission or reflection filters. This requirement has prompted a search for selective filtering coatings with high throughput in the FUV and EUV spectral region. Important progress toward the development of thin film filters with improved efficiency and stability has been made in recent years. The goal for this field is the minimization of absorption to get high throughput and enhancement of wavelength selection.

The development of thin film technology for the FUV and EUV has not progressed as rapidly as visible and infrared technology because substrate and thin film materials exhibit absorption characteristics in these wavelength ranges. As a result of absorption, the optical constant (referred to as the complex refractive index) becomes a complex number. Not only does this complicate the theoretical treatment of the propagation of light across layered media, but it also introduces problems in the determination of the optical constants of thin film and substrate materials.

The Optical Aeronomy Laboratory (OAL) at the University of Alabama in Huntsville has recently developed the technology to determine optical constants of bulk and film materials for wavelengths extending from x-rays (0.1 nm) to the FUV (200 nm) [Zukic, 1989; Zukic and Torr, 1992b; Zukic *et al.*, 1990a, 1992a, 1992b, 1993; Wilson *et al.*, 1993], and several materials have been identified that were used for designs of various optical devices which previously have been restricted to space application in the visible and near infrared [Zukic, 1989; Zukic and Torr, 1991, 1992a, 1992b; Zukic *et al.*, 1990b, 1991, 1992a, 1992b, 1993a, 1993b; Torr *et al.*, 1992; Kim *et al.*, 1992a, 1992b]. A new design concept called the Π-multilayer [Zukic and Torr, 1992b] was introduced and applied to the design of optical coatings for wavelengths extending from x-rays to the FUV. Section 3 explains the Π-multilayer approach and demonstrates its application for the design and fabrication of the FUV coatings.

Two layer Π–stacks have been utilized for the design of reflection filters in the EUV wavelength range from 70-100 nm. Due to the lack of materials with low extinction coefficients very few periods can contribute to interference in this range [Hunter, 1987; Zukic *et al.*, 1991]. Previous EUV instruments were mainly designed as two- or three- mirror imaging systems made

of SiC with a transmission narrowband filter. The transmission filters were deposited either on foils or wire meshes which make them structurally inadequate for most applications. At the same time the EUV transmission filters have a low peak transmittance and a broad passband with insufficient blocking of out-of-band wavelengths [Chiu, 1986; Swift, 1989; Seely and Hunter 1991]. In order to eliminate losses due to the low reflection of the imaging optics and increase throughput and out-of-band rejection of the EUV instrumentation we introduced a self-filtering camera concept [Zukic *et al.*, 1991, 1992b]. The self-filtering approach for the design of the EUV monochromatic imaging systems is described in Section 4 of this chapter.

In the FUV region, MgF_2 and LiF crystals are known to be birefringent [Samson, 1967]. Transmission polarizers and quarterwave retarders made of MgF_2 or LiF crystals are commercially available but the performances are poor. Reflection type polarizers and retarders have also been studied. The Pseudo-Brewster angle of incidence is often used for single boundary reflection polarizers [Hamm *et al.*, 1965] yielding an s-to-p polarization intensity ratio of less than 10. For most polarimetric applications s-to-p ratios of more than 1000 are needed with the s-polarization throughput as high as possible. Similarly, as in the polarizer case, it is possible to find an angle of incidence for a metallic surface at which reflected light has a 90° phase retardance between the s- and p-polarization states [Westerveld *et al.*, 1985; Saito *et al.*, 1990]. Since metals with high FUV reflectance oxidize even in a 10^{-6} torr vacuum (aluminum), single boundary metal surface quarterwave retarders are not suitable for most practical applications. New techniques for the design of the EUV and FUV polarizers and quarterwave retarders are described in Section 5.

X- and γ-ray detectors rely on a measurement of the electron which is ejected when a ray interacts with matter. The design of an x- and γ-ray telescope to operate in a particular region of the spectrum is, therefore, largely dictated by the mechanism through which the rays interact. A telescope is required, not only to detect photons, but also to measure their direction of motion. The direction at which the electron is ejected is only weakly correlated with the direction of the incident photon. Consequently, very little success has been achieved in the construction of high energy detectors with inherent directional sensitivity. Instead, telescopes usually consist of a detector, which merely measures the energy of the x- or γ-ray placed behind some form of collimator. Energy selection and the focusing of the incident high energy rays can be achieved with spectrally selective high reflective multilayers. The design and spectral performance of narrowband reflective x-ray Π-multilayers are presented in Section 6.

A brief review of the theoretical treatment of absorbing multilayers is given in the next section, while our most recent research results are summarized in Section 7 of this chapter.

2.0 ABSORBING MULTILAYER THEORY

The electromagnetic wave absorption of dielectrics is determined by the behavior of bound electrons, while in conducting materials photon interactions with a free electron gas are the main cause of absorption. The theoretical foundation for the mathematical treatment of all absorbing multilayers, regardless of the nature of photon-electron interactions, is based on the assumption that an absorbing material can be treated in the same way as a non-absorbing material if a complex representation of the optical constants is used. The immediate consequence of the complex optical constant representation is that Snell's law does not represent wave refraction, and the ratio c/N does not represent the wave phase velocity. However, by assuming that an incident medium is non-absorbing and by generalizing Snell's law, it is possible to establish a relationship between complex angles in film materials, and the real optical constant and angle in the incident medium. The knowledge of the complex angles within the films and a substrate together with standard matrix multilayer representation provide a powerful tool for the calculation of the layered medium spectral response.

2.1 Matrix Method

In this section we will describe a matrix method followed by Heavens [1965], commonly used to calculate the reflected and transmitted amplitudes of the electric fields of the multilayers. The optical configuration used for this method is shown in Figure 1. The amplitudes of the electric fields of incident wave E_0^+, reflected wave E_0^-, and transmitted wave E_{q+1}^+ are related by the following matrix equation

$$\begin{bmatrix} E_0^+ \\ E_0^- \end{bmatrix} = \frac{C_1 C_2 \cdots C_{q+1}}{t_1 \; t_2 \cdots t_{q+1}} \begin{bmatrix} E_{q+1}^+ \\ E_{q+1}^- \end{bmatrix} \tag{1}$$

for a stratified medium with q layers. C_j is the propagation matrix with the matrix elements

$$C_j = \begin{bmatrix} \exp(i\phi_{j-1}) & r_j \exp(i\phi_{j-1}) \\ r_j \exp(-i\phi_{j-1}) & \exp(-i\phi_{j-1}) \end{bmatrix} \tag{2}$$

where t_j and r_j are the Fresnel transmission and reflection coefficients, respectively, between the (j-1)-th and j-th layers. The Fresnel coefficients, t_j and r_j, can be expressed by using the complex optical constant N_j and the complex refractive angle θ_j. Thus, for s-polarization

$$t_{js} = \frac{2 N_{j-1} \cos \theta_{j-1}}{N_{j-1} \cos \theta_{j-1} + N_j \cos \theta_j} \tag{3}$$

$$r_{js} = \frac{N_{j-1} \cos \theta_{j-1} - N_j \cos \theta_j}{N_{j-1} \cos \theta_{j-1} + N_j \cos \theta_j} \tag{4}$$

and for p-polarization

$$t_{jp} = \frac{2 N_{j-1} \cos \theta_{j-1}}{N_{j-1} \cos \theta_j + N_j \cos \theta_{j-1}} \tag{5}$$

$$r_{jp} = \frac{N_{j-1} \cos \theta_j - N_j \cos \theta_{j-1}}{N_{j-1} \cos \theta_j + N_j \cos \theta_{j-1}} \tag{6}$$

The complex optical constants and the complex refractive angles follow Snell's law

$$N_{j-1} \sin \theta_{j-1} = N_j \sin \theta_j \tag{7}$$

The complex phase thickness is given by

$$\phi_0 = 0 \tag{8}$$

$$\phi_{j-1} = \frac{2\pi}{\lambda} N_{j-1} d_{j-1} \cos \theta_{j-1} \tag{9}$$

where λ is the wavelength of the incident light in vacuum, and d_{j-1} is the physical thickness of the (j-1)-th layer.

Since the final medium is assumed to be semi-infinite, the amplitude of the electric field reflected at q+1 boundary is zero. The amplitude reflectance r and transmittance t are obtained by inserting $E^-_{q+1} = 0$ into Eq. (1), yielding

$$r = \frac{E_0^-}{E_0^+} = \frac{C_{21}}{C_{11}} \tag{10}$$

$$t = \frac{E_{q+1}^+}{E_0^+} = \frac{t_1\, t_2 \cdots t_{q+1}}{C_{11}} \tag{11}$$

where the quantities C_{11} and C_{21} are the matrix elements of the so-called multilayer characteristics matrix C, given by

$$C = C_1\, C_2 \cdots C_{q+1} = \begin{bmatrix} C_{11} & C_{12} \\ C_{21} & C_{22} \end{bmatrix} \tag{12}$$

From the Poynting vector

$$\vec{S} = \frac{c}{4\pi} \vec{E} \times \vec{H}^* \tag{13}$$

and Eqs. (10) and (11) the intensity reflectance R for both polarization states is given by

$$R = |r|^2 \tag{14}$$

and the intensity transmittance T is

$$T_s = \mathrm{Re}\left(\frac{N_s \cos\theta_s}{N_0 \cos\theta_0}\right) |t_s|^2 \tag{15}$$

$$T_p = \mathrm{Re}\left(\frac{N_s^* \cos\theta_s}{N_0^* \cos\theta_0}\right) |t_p|^2 \tag{16}$$

for s- and p-polarization states, respectively. In the above equations, Re indicates the real part of a complex number. The absorptance, A, of a multilayer is given by

$$A = 1 - (R + T) \tag{17}$$

2.2 Electric Field Distribution

Using the matrix method introduced in the previous section, the electric fields in the incident and substrate medium are defined by Eqs. (10) and (11). The electric fields of the inner layers can be calculated from the knowledge of electric fields in either the incident medium or substrate [Apfel, 1986; Ohta *et al.*, 1990]. However, in order to gain a better understanding of the electric field distribution within the Π-multilayers, a more straightforward technique will be introduced. Using this technique the electric fields in a layer can be represented in terms of the electric fields of an adjacent layer and the Fresnel coefficients between those two layers. The advantage of this technique will be demonstrated in the design process of the FUV polarizers and retarders in Section 5.

In Figure 2, E_j is the electric field at the j-th boundary. Subscripts b and t are the bottom and top parts of the boundary, respectively. Superscript + and - are incoming and outgoing waves. There are four different waves at any multilayer boundary; incoming and outgoing waves at the top and bottom of the boundary. For example, E_{jt}^{+} is the sum of all the incoming electric fields at the top of the j-th boundary, while E_{jb}^{-} is the sum of all outgoing electric fields at the bottom of the j-th boundary, and they are related by the following expressions :

$$E_{jt}^{-} = E_{jt}^{+} r_j^{+} + E_{jb}^{-} t_j^{-} \tag{18}$$

$$E_{jb}^{+} = E_{jt}^{+} t_j^{+} + E_{jb}^{-} r_j^{-} \tag{19}$$

where r_j^{+}, r_j^{-}, t_j^{+} and t_j^{-} are the Fresnel reflection and transmission coefficients (Eqs.(3)-(6)), with the same usage of sub and superscripts. Using the relation between Fresnel coefficients,

$$t_j^{+} t_j^{-} - r_j^{+} r_j^{-} = 1 \tag{20}$$

the top electric fields can be expressed as functions of the bottom electric fields :

$$E_{jt}^{+} = \frac{1}{t_j^{+}} \left(E_{jb}^{+} - E_{jb}^{-} r_j^{-} \right) \tag{21}$$

$$E_{jt}^{-} = \frac{1}{t_j^{+}} \left(E_{jb}^{+} r_j^{+} + E_{jb}^{-} \right) \tag{22}$$

The electric fields at the bottom of the (j-1)-th boundary are related to those at the top of the j-th boundary:

$$E^{+}_{j-1\,b} = E^{+}_{jt} \exp(i\phi_{j-1}) \tag{23}$$

$$E^{-}_{j-1\,b} = E^{-}_{jt} \exp(-i\phi_{j-1}) \tag{24}$$

where ϕ_{j-1} is the phase thickness of the (j-1)-th layer. The electric fields at any distance from the j-th boundary are calculated using the phase thickness which corresponds to that distance.

3.0 FUV COATINGS

Narrow-band filters that were commercially available in the FUV wavelength region from 120 nm to 160 nm had a typical transmittance lower than 15% and full width measured at half of the transmittance maximum (FWHM) greater than 25 nm. The peak transmittance of the filters centered at the longer wavelengths from 160 nm - 230 nm was between 20% and 25% with FWHM ≥ 20 nm [Acton 1991]. Malherbe [1974a] reported the design and the spectral performance of a narrow-band filter centered at the Lyman-a (121.6 nm) with peak transmittance close to 15% and FWHM = 9 nm. Blocking of the wavelengths longer than 160 nm was better than 10^{-3}%. The filter had relatively high transmittance for the wavelength region from 126 nm - 135 nm; close to 7% at 126 nm and almost 1% at 135 nm. This pass window renders the filter not very useful for terrestrial imaging applications if spectral discrimination of the neighboring atomic oxygen lines at 130.4 nm and 135.6 nm is desired. A narrow-band filter centered at 202.5 nm was reported by the same author [1974b]. The filter had a peak transmittance greater than 85% and FWHM = 2.5 nm. However, the blocking zone of the filter was very short and the transmittance for wavelengths longer than 220 nm was greater than 85%.

The calculated and experimental spectral performance of a Fabry-Perot-type narrow-band filter centered at 179 nm was reported by Spiller [1974]. His theoretical calculations predicted a narrow-band filter with resolution $\lambda_O/\Delta\lambda$ = 60 and a peak transmittance of 25%, but the measured performance had almost a four times smaller resolution and much smaller peak transmittance. Discrepancies between the theoretically predicted and experimentally obtained spectral curves have been ascribed to the excitation of a surface plasma wave traveling along the surface of an aluminum film.

A variable bandwidth transmission filter reported by Elias [1973] had bandwidths from 7 nm to 20 nm with a peak transmittance from 20% to 40%, respectively. The filter was centered at 176 nm, and as in the case of other all-dielectric filters, suffered from pass windows in the longer wavelength region. Narrowband filters for the FUV wavelength range from 120 nm to 230 nm with similar optical properties to those listed above were also reported by some other authors [Fairchild, 1973; Flint, 1978, 1979; Hunter, 1978 a].

Broadband filters with bandwidths greater than 10 nm, which were available in the FUV had a relatively low transmittance and the shape of the transmittance spectral curve was similar to that of the Fabry-Perot-type filters. For most applications a more rectangular shape for the passband, better out-of-band rejection, and higher transmittance are required [Elias, 1973; Fairchild, 1973; Flint, 1978, 1979; Hunter, 1978a].

Taking all this into account it is obvious that the lack of low absorbing film and substrate materials in the FUV and EUV wavelength regions has prevented design and fabrication of high quality narrow and broadband transmission filters. Realization of spectrally selective FUV and EUV filters with improved performances has required application of Π-stacks for the design and fabrication of high reflective narrowband coatings [Zukic *et al.*, 1991, 1992]. The design approach was to obtain high reflectance by minimizing multilayer absorptance, and by operating in a reflective, rather than in transmissive mode.

3.1 Narrowband High Reflection Filters

In order to explain FUV narrowband filters we start from a Π-multilayer design concept [Zukic *et al.*, 1992a]. For the quarterwave (QW) periodic multilayer case where two film materials have optical thicknesses corresponding to a quarter of a wavelength, it is known that the maximum reflectance of a periodic stack is given by [Koppelmann, 1960]

$$R_k = 1 - 2\pi n_0 \frac{k_H + k_L}{n_H^2 - n_L^2} \qquad (25)$$

where n_H and n_L are refractive indices of high and low index film materials, and k_H and k_L are corresponding extinction coefficients. The ultimate reflectance, R_k, is usually referred to as the Koppelmann limit. It should be emphasized that Eq. (25) is derived with some approximations and it cannot replace an exact calculation of the maximum reflectance of a periodic stack.

Furthermore, for wavelength regions in which the refractive index is less than one, the Koppelmann formula does not give the correct answer for the ultimate reflectance.

The principle of the Π–stack approach is to use a combination of high (H) and low (L) refractive index dielectric pairs so that $H + L = \lambda/2$, where $L/H > 1$, and H and L designate the optical thicknesses of high- and low-index film materials. Since the phase thicknesses of an HL pair add to Π we call stacks made of such pairs Π–stacks or Π–multilayers. Thus a quarterwave stack (QW; optical thicknesses of layers are $\lambda/4$) is a special case of Π-multilayers with $L/H = 1$. In a QW stack the light that is reflected from all interfaces is in phase, while in a Π multilayer the light that is reflected from each HL pair is in phase. Obviously, QW stacks with low-absorbing film materials (which are available in visible and infrared parts of the spectrum) provide higher reflectance with fewer layers than other Π-stacks. However in the FUV and EUV where low-absorbing high-index film materials do not exist, a Π-multilayer with a smaller physical thickness of H relative to L provides lower absorptance and therefore higher reflectance of the stack [Zukic and Torr, 1991, 1992a].

Figure 3 shows maximum reflectance as a function of the L/H ratio of a 35-layer reflection filter designed for 145 nm using MgF_2 and LaF_3. The reflector has a maximum reflectance when the ratio $L/H = 3$. This corresponds to the optical thickness of $L(MgF_2) = 3\lambda/8$ and $H(LaF_3) = \lambda/8$. The Koppelmann limit (QW stack; $L/H = 1$) for this design is 89.6%.

As the optical thickness ratio (L/H) of the Π-multilayer changes the high reflectance bandwidth or so-called full width at half of the reflectance maximum (FWHM) also changes. This property is used to control the high reflectance bandwidth of the filter. Figure 4 shows the bandwidth of the 35-layer stack designed for 145 nm using MgF_2 and LaF_3 as a function of L/H ratio. It is obvious that for the design of a narrowband reflector ratio L/H has to be as high as possible. However, an increase of the L/H ratio requires the addition of more layers to the stack in order to maintain reflectance at its design maximum. Furthermore, the value of the L/H ratio and therefore the minimum thickness of an H layer is certainly limited by the feasibility of depositing and monitoring extremely thin layers. Other important factors that limit the maximum value of the L/H ratio include a substrate surface roughness and structural properties of the layers.

The Π-multilayer approach was utilized for the design and fabrication of narrowband and broadband FUV filters for NASA's ultraviolet imager (UVI) which is the part of the International Solar-Terrestrial Physics (ISTP) mission [Zukic *et al.*, 1992a; Torr *et al.*, 1992; Torr *et al.*,

1993]. The ISTP imager is designed to image four features of the aurora: OI lines at 130.4 nm and 135.6 nm and the N_2 Lyman-Birge-Hopfield (LBH) bands between 140 nm -160 nm (LBH short) and 160 nm-180 nm (LBH long). Narrow-band filters designed and fabricated for the OI lines have a bandwidth of less than 5 nm and a peak transmittance of 22.3% and 29.6% at 130.4 nm and 135.6 nm, respectively. Broadband filters designed and fabricated for LBH bands have transmittance greater than 60% for both LBH short, and LBH long. Blocking of out-of-band wavelengths for all filters is better than 10^{-3}% with the transmittance at Lyman α 121.6 nm line of less than 10^{-6}% [Zukic *et al.*, 1992a].

Figure 5 shows the measured net transmittance through three 130.4 nm Π multilayer narrowband reflection filters combined with a transmission filter. Reflection filters are mounted in the filter box together with the transmission filter. The peak transmittance of the combination is greater than 22.3% with 4.5 nm bandwidth. Figure 6 shows the measured net transmittance through three narrowband reflection filters centered at 135.6 nm combined with a cut-on transmission filter. The reflection filters are 35-layer Π stacks with $H = \lambda/8$, and $L = 3\lambda/8$. The transmission filter is a BaF_2/MgF_2 2-layer stack on a MgF_2 substrate. The peak transmittance of the filter combination is 29.6% with 5 nm bandwidth.

3.2 Broadband High Reflection Filters

The pass zone of a broadband filter is bounded by a lower and upper wavelengths. Ideally, the spectral components of the incident light with wavelengths shorter than the lower and longer than the upper wavelength of the filter, together referred to as the out-of-band spectrum, are rejected. In the design examples that follow, wavelengths of the out-of-band spectrum are rejected by means of multiple reflections from QW stacks. The rejection at shorter wavelengths might be improved by the suitable choice of the window material, placed at the entrance of a multi-reflector combination. Windows made of BaF_2 and CaF_2 absorb wavelengths below 135 nm, and 125 nm respectively, while Fused Silica and aluminum oxide may be used for broadband filters with a lower pass limit above 145 nm [Zukic *et al.*, 1990a].

Due to the narrower high reflection zone, the Π multilayers with $L/H > 1$ are not suitable for the design of broadband reflectors. A QW stack for which $L/H = 1$ is a better choice for the design and fabrication of these filters. Figure 7 shows the measured net transmittance through the combination of three reflection filters designed for LBH short FUV bands, using a BaF_2 substrate with protective MgF_2 coating as the transmission filter. The filter combination has a peak transmittance of more than 60% and a bandwidth of 11 nm. Figure 8 shows the measured

net transmittance through the filter combination designed for the LBH long FUV bands. The combination comprises three reflection filters, and a bare Fused Silica substrate as the transmission filter. The filter combination has a peak transmittance close to 60% and a bandwidth of 11 nm. The average rejection of the out-of-band spectrum up to 2500 nm is better than $4 \times 10^{-4}\%$ with the transmittance for wavelengths below 150 nm of less than $10^{-6}\%$.

3.3 FUV Transparent Conductive Coatings

In many cases a space-borne optical instrument with a dielectric window requires a conductive transparent coating deposited on the window to remove the electrostatic charge collected due to bombardment of ionized particles. We have fabricated conductive coatings on the MgF_2 window of the ISTP imager with FUV transmittance higher than 40% and resistance lower than 800 Ω [Kim *et al.*, 1993].

Figure 9 shows the measured transmittance of two FUV transparent conductive coatings deposited on MgF_2 substrates. The solid line represents a conductive coating which has 6500 Ω/cm^2 resistance with FUV transmittance greater than 50% for all wavelengths above 125 nm. The dashed line represents a conductive coating with less than 800 Ω/cm^2 resistance and more than 45 % transmittance for $\lambda > 125$ nm.

4.0 EUV AND FUV POLARIZERS AND RETARDERS

4.1. Reflection Quarter Wave Retarder (QWR)

It is known that in the FUV region, a LiF and MgF_2 crystal can act as a retarder when pressure is applied to the edges of the crystal [Samson, 1967]. LiF has a lower absorption edge than MgF_2, but hygroscopic properties cause severe problems with respect to transmission in the practical use of LiF plates [Winter *et al., 1987*]. Saito *et al.* [1990] stated that two MgF_2 plates with orthogonal optical axes and optical path lengths differing by a quarter wavelength (Δd = 6.85 mm) can act as a QWR. However, there is a steep change in the phase difference between 115 - 130 nm.

There have been several studies using metallic surfaces as QWRs. Saito *et al.* [1990] found a phase difference change of 40°, centered about 90° over the entire spectral range of 90-180 nm for an aluminum mirror. However, aluminum mirrors tend to oxidize and make an Al_2O_3 layer [Smith *et al.*, 1985]. The Al_2O_3 film has high absorption below 170 nm, reducing

the reflectance of the aluminum in this region [Gervais, 1991]. Westerveld *et al.* [1985] found that Au surfaces can give a 90° phase difference at 57.5° angle of incidence for 55-125 nm and at 62.5° for 120-200 nm. They adjusted the angle representing the orientation of the electric vector of the incident light with respect to the plane of incidence to make the reflectances equal for s- and p-polarizations. In contrast to a single metallic surface, a multilayer reflection retarder provides the freedom to specify both the incident angle and the retardance value as well as high and matched reflectances for both polarization states.

A multilayer that satisfies the following requirements imposed on reflectance and phase is known as a QWR

$$|r_s| = |r_p| \tag{26}$$

$$\Delta\phi = |\phi_s - \phi_p| = 90° \tag{27}$$

i.e.,

$$\frac{r_s}{r_p} = \pm i \tag{28}$$

In addition to the basic requirement given by Eq. (28), a QWR needs to have high reflectance, be insensitive to small changes of wavelength, and be convenient for the practical applications.

In order to achieve the basic QWR requirement, namely Eq. (28), with a high reflectance, we need a pair of high and low absorbing film materials. The Fresnel reflection coefficients (Eqs. 3-6) have large amplitudes for s- and p-polarizations, and a large phase difference between the two polarizations at a boundary between high and low absorbing materials. Aluminum and MgF_2 film materials satisfy the high-low absorptance boundary requirement for the wavelength range extending from 110 nm - 200 nm. At 121.6 nm, the reflectance from a single boundary between these two film materials gives a 26.9° phase difference for light coming in from vacuum at a 45° angle of incidence. Thus, if the phase retardance remains close to 30° for a single boundary reflectance, then at least three high-low boundaries in the multilayer are needed to achieve quarter wave retardance. Consider now a MgF_2/Al/MgF_2 three-layer structure which together with an aluminum substrate provides 3 high-low absorptance boundaries.

As mentioned earlier, aluminum and MgF_2 were selected as film materials because of their respective high and low FUV absorptance. However, the central Al layer should be as thin as possible to avoid large losses due to absorption. The design task then becomes that of determining the thicknesses of the two MgF_2 layers that will yield the best performance.

At the first boundary, the incident amplitude $E^{+}_{1\,t}$ is always 1, and the reflected amplitude $E^{-}_{1\,t}$ is defined by the reflectance and basic QWR requirements given by Eq. (28). Starting with these two known values, the electric fields at the top of the 4-th boundary $E^{+}_{4\,t}$ and $E^{-}_{4\,t}$ can be calculated using Eqs. (21)-(24). In addition these two fields are related by Eq. (18), thus providing a system of two equations with two unknowns; one for each polarization sate:

$$\begin{aligned} & e^{i(\phi_1+\phi_2)}\,(r_{s/p}-r_{12})\left(e^{i\delta}-r_{23}^2\,e^{-i\delta}\right) \\ & +e^{-i(\phi_1+\phi_2)}\,(1-r_{s/p}\,r_{12})\left(r_{23}^3\,e^{i\delta}-r_{23}\,e^{-i\delta}\right) \\ & +e^{i(\phi_1-\phi_2)}\,(r_{s/p}-r_{12})\,r_{23}^2\left(e^{-i\delta}-e^{i\delta}\right) \\ & +e^{-i(\phi_1-\phi_2)}\,(1-r_{s/p}\,r_{12})\,r_{23}\left(e^{-i\delta}-e^{i\delta}\right)=0 \end{aligned} \qquad (29)$$

where $r_{s/p}$ is the target amplitude reflectance for the s- and p-polarizations, r_{12} and r_{23} are the Fresnel reflection coefficients at the vacuum/MgF_2 boundary and the MgF_2/Al boundary, respectively, and δ is the phase thickness of the central Al layer. The two unknowns, ϕ_1 and ϕ_2 are the phase thicknesses of two MgF_2 layers.

These equations can be easily solved by numerical fitting with an additional optimization of the thickness of the aluminum film [Zukic, 1984]. Figure 10 shows the calculated electric fields at the top and the bottom of each boundary for the MgF_2/Al/MgF_2 /Al-substrate design. In the figure, the length of a straight line represents the amplitude, and the direction of a line represents the phase angle of the electric field relative to the incident wave. It shows the 90° phase difference between reflected waves of the two polarizations. 90° phase changes are seen in the two MgF_2 layers, and no change in Al layer. It also shows that the sum of the tangential components of the electric fields are continuous at the every boundary. It is assumed in this calculation that r_S = (0, i 0.8), r_p = (0.8, 0), and $\phi_1=\phi_2\sim\pi/2$.

Figure 11 shows the calculated performance of the QWR designed for the Lyman-α line at 45° angle of incidence. It has 81.05% reflectance for the s-polarization case and 81.04% for the p-polarization case, and the phase difference between these two polarizations is 90.07°. In the FUV region, all film materials are affected by dispersion, and therefore only a narrow wavelength region can be optimized for high reflectance and 90° phase retardance. Utilizing the same approach and the same film materials, three layer QWR structures can be designed for the entire FUV region and for 100-120 nm part of the EUV spectrum. When MgF_2 and aluminum are used for the 3-layer structure QWR designs for the shorter wavelength region of the EUV, they exchange roles; MgF_2 has to be used as high, and aluminum as low absorbing material.

4.2 Reflection Polarizers

In the FUV region, a MgF_2 crystal is known to be birefringent for the wavelengths above 130 nm [Samson, 1967]. Johnson [1964] reported a MgF_2 transmission polarizer with 40% transmittance for $\lambda < 160$ nm which then dropped to zero near 120 nm. Winter and Ortjohann [1987] used a 'pile-of-plates' transmission polarizer made of four MgF_2 crystal plates for the Lyman-α line (λ=121.6 nm). The transmittance was 20% and the polarization efficiency (Rs-Rp)/(Rs+Rp) was 85±1%. Other authors reported that very high polarization efficiency can be achieved when incident radiation is reflected from crystals [McIlrath, 1978; Saito *et al.*, 1990; Hass and Hunter, 1978]. Although almost complete polarization was achieved when crystals are oriented at the Brewster angle, the polarizers have limited practical application because of very low throughput for s-polarization. In this section we will explore the possibility of application of the so-called induced transmittance effects to the design of thin film reflection polarizers.

Berning and Turner [1957] showed that a reasonably thick metal film can be induced to transmit a surprising amount of energy of a particular wavelength when it is surrounded by suitably chosen interference film combinations. They called this technique induced transmission and applied it to a bandpass filter design. The induced transmittance concept can be used for the design of the FUV polarizers [Kim *et al.*, 1992]. The first step in this approach is the design of a multilayer which has a very low p-polarization reflectance. This can be achieved by inducing transmission and absorption for p- while maintaining a large reflectance for s-polarization. Again, MgF_2 and aluminum are used to design a MgF_2/Al/MgF_2/Al-substrate three-layer structure which induces transmittance and absorptance for p, and provides high reflectance for s polarization.

The top MgF_2 layer induces p-polarization transmission into the aluminum layer. With the help of this top MgF_2 layer, some of the p-polarization light is absorbed while the rest makes it through to the bottom MgF_2 layer. The bottom MgF_2 layer further induces p-state transmission into the substrate and increases transmittance into Al film for the p-polarization component reflected from the substrate surface. Because of the large differences of the Fresnel transmission and reflection coefficients, these two MgF_2 layers work differently for the s-polarization state.

The optimum thicknesses of the films in the MgF_2/Al/MgF_2 structure were determined by the summation method [Heavens, 1965]. Using this method we can trace step by step every reflected and transmitted wave, and select important reflected waves. Important waves are those

which have much larger amplitudes than other waves at a specific point. By considering the phase difference between important waves the optimum $MgF_2/Al/MgF_2$ design can be selected.

Figure 12 shows the light waves used to determine the thin film thicknesses. Table 2 shows the Fresnel reflection and transmission coefficients for the p-polarization state when the light is incident from vacuum at a 45° angle of incidence. To determine the thickness of the top MgF_2 layer, we consider 'a' and 'b' as important waves in Figure 12. The other waves that reach the second boundary from above are much weaker than these two since the amplitude of the Fresnel reflection coefficient at MgF_2/vacuum boundary is 0.14, as shown in Table 2. In order to make the top MgF_2 layer a transmission induced layer, 'a' and 'b' must interfere destructively. Then these waves can pass through the central Al layer with very little absorption. The wave 'b' passes through the top MgF_2 layer twice, and is reflected at the first and second boundary after it starts from 'a'. The thickness of the top MgF_2 layer is determined to make the sum of the phase changes of this round trip equal to π.

Table 2. The Fresnel reflection and transmission coefficients for p-polarization light incident at a 45° angle of incidence from vacuum. Top: amplitude ratio of the reflected or transmitted light to the incident light; Bottom: phase change.

Incident Material	Reflection at Boundary			Transmission at Boundary		
	Vacuum	MgF_2	Al	Vacuum	MgF_2	Al
Vacuum		0.14 (+178.6)			0.67 (+0.3)	
MgF_2	0.14 (-1.4)		0.96 (+54.5)	1.47 (-0.3)		1.35 (+27.1)
Al		0.96 (-125.5)			1.16 (-60.8)	

The bottom MgF_2 layer works as a transmission and absorption induced layer for the p-polarization. In order to induce absorption, the sum of the waves going up to the central Al layer must have a large amplitude. This is achieved by making the waves interfere constructively. For this purpose, we consider the 'd' and 'e' waves as important waves. The amplitudes of the transmission coefficient are 1.16 and 1.35 at the Al/MgF_2 and MgF_2/Al boundaries, respectively. The reflection coefficient at MgF_2/Al is 0.96. The decrease in amplitude by propagation through the MgF_2 layer is small. Therefore, 'd' and 'e' have larger amplitudes than 'c'. Furthermore, the multiply reflected waves 'f', 'g', ··· can be made in phase with 'd' and 'e'. For the transmission induced layer, 'h' and 'i' waves are important. If we make them interfere constructively, they will

have large amplitudes when they go into the substrate. As a result, this three layer structure has a large transmittance for p-polarization. The constructive interference between 'd' and 'e', and between 'h' and 'i' are achieved simultaneously, because the bottom MgF_2 layer is sandwiched by Al. The phase differences between 'd' and 'e', and 'h' and 'i' are equal. The thickness of the bottom MgF_2 layer is chosen to make the phase difference equal to zero. Consequently, the bottom MgF_2 layer thickness is approximately half that of the top MgF_2 layer.

The exact thicknesses of the two MgF_2 layers and the best thickness of the central Al layer are determined by numerical computer fitting [Zukic, 1984]. Figure 13 shows the changes of the electric fields for a polarizer designed for the Lyman-α line at a 45° angle of incidence. The electric fields at the top and bottom of each boundary in the three layer thin film are calculated by the method explained in section II-C. The length and the direction of the line are the amplitude and the phase angle representation of the electric field relative to the incident wave. From Figure 13, it can be seen that with the help of the top MgF_2 layer, most of the p-polarized wave passes through the high absorbing Al layer. The figure also shows that the bottom MgF_2 layer acts as a transmission and absorption induced layer. The p-polarization transmittance and absorptance are 34.50% and 64.29%, respectively, while s-polarization has 0.97% transmittance and 10.36% absorptance.

Figure 14 shows the calculated spectral performance of the polarizer designed for the Lyman-α line, at a 45° angle of incidence. The design has a 88.67% reflectance for the s-polarization case, and a 1.21% reflectance for the p-polarization case. The polarization efficiency p = (Rs-Rp)/(Rs+Rp) is 97.31%. Utilizing multiple reflections from these 3-layer structures polarizers with polarization efficiency of more than 99% and 60% net throughput for s-polarization can be designed for the entire FUV region. Figure 15 shows degree of polarization calculated for the single, double, and triple reflection for the polarizer shown in Figure 14.

5.0 EUV COATINGS

Optical instrumentation used for EUV line observations lacks high quality narrowband filters and high reflectance mirrors, and even now available coating and detector technology would not provide observations at EUV wavelengths with desirable signal-to-noise ratios. Previous EUV instruments were mainly designed as two- or three - mirror systems made of SiC with a transmission narrowband filter. Currently available transmission filters have a low peak transmittance, and broad pass band without sufficient blocking of out-of-band wavelengths [Chin *et al.*, 1986, 1990; Swift *et al.*, 1989].

For example, the SiC mirror has less than 30% reflectance at 83.4 nm, thus, for a three-mirror imaging instrument, the transmission without the filter is 2.7%. Currently available narrowband filters centered at 83.4 nm have a transmittance of less than 15% [Chakrabarti, 1991] which yields less than 0.34% for the total transmission of the instrument. Taking into account the low out-of-band rejection, it becomes obvious why such instruments yield marginal signal-to-noise ratios for relatively weak terrestrial EUV emissions. Due to the lack of high reflectance coating materials in the EUV, most instrumentation intended for imaging at shorter EUV wavelengths, such as 30.4 nm utilizes a grazing incidence configuration. Chakrabarti *et al.* [1990] reported the design of a multilayer coating which had almost 25% reflectance for near zero angles of incidence at 30.4 nm. In spite of this relatively high reflectance, a two-mirror imaging system would have throughput close to 6%, while a three-mirror system, which might be more desirable for higher quality imaging, would have throughput of less than 1.5%. Taking into account that currently available narrowband filters centered at 30.4 nm have a peak transmittance close to 16% [Chakrabarti, 1991], it is clear that imaging systems at 30.4 nm will have a throughput of less than one percent. Currently available narrowband filters for 121.6 nm have a bandwidth of more than 15 nm and a peak transmittance of less than 10% [Acton, 1991]. Blocking of out-of-band wavelengths is not better than 0.1%. For most applications a much narrower bandwidth and better rejection for out-of-band wavelengths is needed.

As in the case of the FUV region, EUV filters with improved spectral performance were obtained by using the Π-stack design concept [Zukic *et al.* 1991, 1992]. The design approach obtains high filter throughput by minimizing energy loss in the filters and by operating in a reflective, rather than in transmissive, mode. In order to maximize the throughput of a candidate EUV camera/telescope design we used the instrument imaging mirror surfaces as narrowband reflective filters. Since the mirrors provide both the imaging and spectral filtering we introduced the terminology "self-filtering" to depict the instrument design concept for EUV applications [Zukic *et al.*, 1991]. An important aspect of our design is the insensitivity of our coatings to cone angle of the incident radiation. This is another critical design feature if the self-filtering approach is to work.

Figure 16 shows the calculated spectral reflectance of the 83.4 nm reflection filter designed for the angular cone of 30° ± 20°. We have fabricated the filter in a conventional high vacuum chamber (10^{-7} torr < p < 10^{-6} torr) using fast deposition rates to minimize the oxidation of the aluminum film. This approach limits our ability to control the layer thicknesses, resulting in shifts in the peak reflectance wavelength and broadening of the response feature. The

measured spectral performance of the fabricated filter for angles of incidence of 10°, 30°, and 50° are shown in Figure 17. Since the spectrophotometer used to measure the filter response could not measure wavelengths below 65 nm, the measured values are given from 65 nm - 100 nm. The peak reflectance is shifted toward shorter wavelengths, but the intensity is very close to the theoretical prediction. Lower deposition rates and accurate thickness control could be achieved if the filters were deposited in an ultra high vacuum coater.

Figure 18 shows the throughput of a three mirror camera/telescope when mirror surfaces are coated with the narrowband reflective coatings shown in Fig. 16. Incident light after three reflections will reach the image plane with less than 0.1% of out-of-band radiation, and more than 20% of in-band radiation. The overall transmission of the three-filter combination is calculated as the average over angles of incidence. The calculated peak transmission of the filter combination at 83.4 nm is greater than 20% with less than 7 nm bandwidth, and average out-of-band transmission less than 0.1%. The filter combination transmission at 30.4 nm and at 58.4 nm is 0.03%, and 0.05%, respectively. The calculated transmission at 121.6 nm is 0.004%.

Figure 19 shows the throughput of a 58.4 nm three mirror self-filtering camera/telescope, and a single reflection from a SiC/MgF_2 Π multilayer. The superiority of the self-filtering camera/telescope becomes apparent when compared to previously designed systems [Seely and Hunter, 1991; Chakrabatri, 1991] which yielded transmissions of less than 1%. Utilizing the self-filtering approach instruments with similar performances are possible for imaging at other EUV wavelengths such as the He II 30.4 nm feature.

6.0 X-RAY COATINGS

At x-ray and gamma ray frequencies the energy carried by a single photon is very large and the number of photons in a beam of a given energy flux is correspondingly small. The statistical fluctuations in the total number of photons detected, both in the signal and in the background radiation, are thus the overriding factor in the sensitivity of x- and γ-ray telescopes. Since it is difficult to construct a detector for high energy radiation which is inherently directional in its sensitivity, measurements on localized sources require some form of collimation to distinguish between the parallel, or nearly parallel, beams of radiation from sources and the much larger diffuse flux of background radiation. When an active or passive shield is used around a detector it may also be made to serve as a collimator simply by extending it in the forward direction. However, in all space experiments, whether on balloons, rockets, or satellites,

the total weight of the telescope is an important factor which limits the size and weight of the collimating system.

Spectrally selective highly reflective interference multilayers can provide information on both the energy of the incident radiation and its direction. Energy selection and the focusing of the incident high energy x- and γ-rays can be achieved, in a way similar to what has been done in the EUV region. If optical imaging surfaces of a telescope are coated with a narrowband reflecting multilayer then a very narrow spectral band of incident radiation will reach detector, thus providing both imaging and spectral filtering. The high reflective multilayers in future x-ray telescopes would replace the thick and heavy collimator and/or grating materials.

The calculated reflectance of an x-ray narrowband reflective multilayer for two different angles of incidence is shown in Figure 20. The calculated reflectance for 80° angle of incidence shows a reflectance peak value of 35.8% at 0.73 nm (2.621 KeV) with the bandwidth of the reflector less than 0.01 nm. The in-band to out-band ratio is more than 3000, with an instrument monochromatic sensitivity factor $T[\%]/\Delta\lambda[nm] > 3600$. At 85° angle of incidence the peak reflectance is more than 65% at 0.44 nm with a bandwidth of less than 0.006 nm providing the ratio $T[\%]/\Delta\lambda[nm] > 10{,}000$. This design provides very high spectral purity with reflectances as high as 65% for angles of incidence between 80° and 85°. Using the same design approach x-ray filters with similar spectral performance can be obtained for the entire wavelength range from 0.1 nm - 7.0 nm. These non-grazing high reflective narrowband filters together with the self-filtering approach will result in a new generation of x-ray telescopes replacing current telescope designs based on large and heavy collimators and gratings.

7.0 COATINGS AND SPACE ENVIRONMENT

Since the early sixties there has been considerable interest in the behavior of optical materials, and optical thin films in the hostile space environment. Heath and Sacher [1965, 1966] reported on the effects of a simulated high energy electron space environment on the ultraviolet transmission of LiF, MgF_2, CaF_2, BaF_2, Al_2O_3, and SiO_2. They found that the transmittance of MgF_2, and BaF_2 did not change significantly in the EUV and FUV (105 nm - 180 nm) even after being exposed to flux of 10^{14} electron/cm^2 with electron energies from 1 MeV and 2 MeV. High energy protons from solar flares and in the inner Van Allen belt are an important component of the space radiation environment for near-earth orbits. Protons with energies of several hundred MeV are of particular concern because they may produce nuclear reactions and spallation products that lead to induced radioactivity in irradiated materials. Reft *et*

al. [1980] reported on proton induced degradation of the FUV (105 nm - 210 nm) transmittance of LiF, and MgF_2. The proton fluence was $2.8x10^{13}$ proton/cm^2, with energies of 85 MeV and 600 MeV. It was found that MgF_2 is substantially more radiation resistant than LiF in the FUV, and therefore more suitable for space applications.

Gillette and Kenyon [1971] found that radiation induced degradation of MgF_2 overcoated Al mirrors is negligible. In 1970 Hass and Hunter reported on the effects of electron, proton, and UV irradiation on the reflectance of the EUV and FUV mirrors. Their results agree with reports of other authors (referenced above) that MgF_2 overcoated Al mirrors are radiation resistant. According to the research conducted by many authors, and from our own experience [Keffer *et al.*, 1993] it may be concluded that Al, and MgF_2 are suitable as film materials for space applications. In addition to these two materials, BaF_2 together with SiO_2, were found to be resistant to the high energy radiation of the space environment.

The hazardous effects for coatings and substrates during the exposure to the low Earth orbit space environment are erosion, surface and volume contamination, and structural-chemical changes of film and substrate materials. The most likely cause of erosion is bombardment by atomic oxygen while surface and volume contamination and structural changes may be caused by a number of different environmental effects.

Figure 21 shows computer modeling of erosion effects on the EUV narrowband reflective coating previously shown in Figs. 16 and 17. The reflectance change caused by erosion is only modeled for 30° angle of incidence. The computer modeled erosion is stopped at the point when both outer layers of Ge and MgF_2 are eroded away (step S1 in Fig. 21). At this point we assume that the coating will then be exposed to two combined effects: erosion and aluminum oxidation, i.e. chemical change of the film. Assuming different rates for erosion and oxidation one can end with a number of surprising results. Step S2 in Figure 21 shows computer modeling of how erosion and oxidation combined together further degrade the spectral performance of the EUV filter. It is assumed, in the computer model, that the aluminum film oxidizes at a much faster rate than it erodes.

Other sources of structural-chemical changes of film and bulk materials are high energy radiation and heat absorption. Since some of our materials have already been tested in high energy space environment simulators we do not expect significant structural-chemical changes for BaF_2, MgF_2, LaF_3, and Al by high energy radiation. However, high energy radiation combined say with erosion and volume contamination might provide completely different answer

to the high energy radiation damage threshold even for those well known and many-time tested materials.

We expect that surface contamination will be at its highest level during engine and thruster firings or any other vehicle or payload activity which may create contaminants. The volume contamination which is caused by inclusion of foreign molecules in film and substrate materials might also increase during the vehicle and payload activities in soft film and substrate materials.

Step S3 shows computer modeling of further degradation of the EUV multilayer caused by adding surface contamination to erosion and oxidation. It is assumed that erosion is still a much slower process than surface contamination and oxidation. The surface contaminant used in the calculation is modeled as a gradient index film with extinction coefficient exponentially dependent on the film thickness, and increasing in value with wavelength. This explains the relatively high reflectance of the coating in the step S3 in longer wavelength regions, where the contaminant acts as a reflective film. In the steps S4 and S5 we combined erosion, oxidation and surface contamination effects at the same rate. From the reflectance calculations in steps S4 and S5, it seems that contaminant would not go away easily .

8.0 SUMMARY

The improved FUV filters that we have designed and fabricated were made as combinations of three reflection and one transmission filter. Narrowband filtering with a bandwidths of 5 nm and a throughput at the central wavelength of more than 20% is achieved, for example, at 130.4 nm and 135.6 nm with the average blocking of out-of-band wavelengths of better than $4 \times 10^{-4}\%$. In the case of broadband filters a multiple reflector centered at 150 and 170 nm combined with corresponding transmission filters had a bandwidth of more than 11 nm and the transmittance greater than 40% and close to 60%, respectively. The average blocking of out-of-band wavelengths is better than $4 \times 10^{-4}\%$. The idea of utilizing the multiple reflections from Π multilayer reflectors constitutes the basis of the design approach used for the narrowband and broadband filters. The multiple reflector combinations provide spectral performance for narrow and broadband filters superior to what was previously available.

A new technique for the design of FUV polarizers and retarders are presented. The 3-layer QWR structure designed provides high reflectances for s- and p-polarizations and a phase retardance close to 90°. A concept of induced transmission and absorption together with layer-

by-layer electric field calculation was utilized to design a multilayer reflection polarizer in the FUV region. Using MgF_2 and Al as a low absorbing and a high absorbing materials pair high s-polarization reflectance and a high polarization efficiency were achieved.

The idea of utilizing imaging mirrors as narrowband filters constitutes the basis of the design of extreme ultraviolet imagers operating at 58.4 nm and 83.4 nm. The net throughput of both imaging-filtering systems is better than 20%. The superiority of the EUV self-filtering camera/telescope becomes apparent when compared to previously theoretically designed 83.4 nm filtering-imaging systems which yielded transmissions of less than 1% [Seely and Hunter, 1991], and therefore less than 0.1% throughput when combined with at least two imaging mirrors. Utilizing the self-filtering approach instruments with similar performances are possible for imaging at other EUV wavelengths, such as 30.4 nm. The self-filtering concept can be extended to the x-ray region where its application can result in the new generation of x-ray telescopes which could replace current designs based on large and heavy collimators.

9.0 REFERENCES

Acton Research Corporation, **Optical Filters**, Catalog (1991).

Chakrabarti, S., R. Kimble, and S. Bowyer, "Spectroscopy of the EUV(350-1400 Å) nightglow", **J. Geophys. Res. 89**, 5660 (1984).

Chakrabarti, S., J. Edelstein, R. A. M. Keski-Kuha and F. T. Threat, "An 834 Å reflective coating for magnetospheric imagery applications", **Proc. SPIE Vol. 1744**, 208 (1992).

Chin, Y. T., R. M. Robinson and G. R. Swenson, "Imaging the flow of ionospheric ions into the magnetosphere", **Nature 322**, 441 (1986).

Chin, Y. T., R. M. Robinson, W. L. Collin, S. Chakrabarti and G. R. Gladstone, "Magnetospheric and exospheric imaging in the extreme ultraviolet", **J. Geophys. Res. 17**, 267 (1990).

Elias, L. R., R. Flach and W. M. Yen, "Variable bandwidth transmission filter for the vacuum ultraviolet: $La_{1-x}Ce_xF_3$", **Appl. Opt. 12**, 138 (1973).

Fairchild, E. T., "Interference filters for the VUV (1200-1900 Å)", **Appl. Opt. 12**, 2240 (1973).

Flint, B. K., "Special application coatings for the vacuum ultraviolet (VUV)", **Opt. Eng. 18**, 92 (1979).

Flint, B. K. , "Special application coatings for the vacuum ultraviolet", **Proc. SPIE Vol. 140**, 131 (1978).

Gillette, R. B., and B. A. Kenyon, "Proton-induced contaminant film effects on ultraviolet reflecting mirrors", **Appl. Opt. 10**, 545 (1971).

Hamm, R. N., R. A. MacRae and E. T. Arakawa, "Polarization studies in vacuum ultraviolet", **J. Opt. Soc. Am. 55**, 1460 (1965).

Hass, G., and W. R. Hunter, "Laboratory experiments to study surface contamination and degradation of optical coatings and materials in simulated space environment", **Appl. Opt. 9**, 2101 (1970).

Hass, G., and W. R. Hunter, "Reflection polarizers for the vacuum ultraviolet using Al+MgF_2 mirrors and MgF_2 plate", **Appl. Opt. 17**, 76, (1978).

Heath, D. F. and P. A. Sacher, "Effects of a simulated high energy electron space environment on the ultraviolet transmittance of optical materials between 1050 and 3000 Å", **NASA Report X-622-65-382** (1965).

Heath, D. F. and P. A. Sacher, "Auger spectroscopy examination of MgF_2-coated Al mirrors before and after UV irradiation", **Appl. Opt. 5**, 937 (1966).

Hunter, W. R., "Review of vacuum ultraviolet optics", **Proc. SPIE Vol. 140**, 122 (1978a).

Hunter, W. R., "Design criteria for reflection polarizers and analyzers in the vacuum ultraviolet", **Appl. Opt. 17**, 1259 (1978b).

Johnson, W.C., "Magnesium fluoride polarizing prism for the vacuum ultraviolet", **Rev. Sci. Instrum. 35**, 1375 (1964).

Keffer, C. E., M. R. Torr, M. Zukic, J. Spann, D. G. Torr and J. Kim, "Radiation damage effects in FUV filters and substrates", to be presented at **SPIE** conference on Optical Materials, San Diego, California, 11-16 July (1993).

Kim, J., M. Zukic and D. G. Torr, "Multilayer thin film designs as far ultraviolet polarizers", **Proc. SPIE Vol. 1742**, in press (1992a).

Kim, J., M. Zukic, J. Park, C. Keffer and D. G. Torr, "Optical constants of ITO, NiCr, Cr, and Mg conductive coatings in the far ultraviolet", to be presented at **SPIE** conference on Instrumentattion for Magnetospheric Imagery, San Diego, California, 11-16 July (1993).

Kim, J., M. Zukic, D. G. Torr and M. Wilson, "Multilayer thin film designs as far ultraviolet retarders", **Proc. SPIE Vol. 1742**, in press (1992b).

Malherbe, A., "Interference filters for the far ultraviolet", **Appl. Opt. 13**, 1275 (1974a).

Malherbe, A., "Multidielectric components for the far ultraviolet", **Appl. Opt. 13**, 1276 (1974b).

Malaguti, G., A. J. Bird, E. Caroli, A. J. Dean, G. D. Cocco, B. M. Swinyard and G. E. Villa, "The imaging and spectroscopy capabilities of the integral imager: Monte-Carlo simulation results", **AIP Conf. Proc. 232**, 489 (1990).

McIlrath, T. J., "Circular polarizer for Lyman-α flux", **J. Opt. Soc. Am. 58**, 506 (1968).

Reft, C. S., J. Becher and R. L. Kernell, "Proton-induced degradation of VUV transmission of LiF and MgF_2", **Appl. Opt. 19**, 4156 (1980).

Saito, T., A. Ejiri and H. Onuki, "Polarization properties of an evaporated aluminum mirror in the VUV region", **Appl. Opt. 29**, 4538 (1990).

Samson, J. A. R., **Techniques of Vacuum Ultraviolet Spectroscopy**, Chap. 9, John Wiley & sons, New York, (1967).

Seely, J. F., and W. R. Hunter, " Thin film interference optics for imaging the O II 834-Å airglow", **Appl. Opt. 30**, 2788 (1991).

Spiller, E., "Multilayer interference coatings for the vacuum ultraviolet", in **Space Optics**, B. J. Thompson and R. R. Shanon, eds., Proc. of the Ninth International Congress of the International Commission for Optics, National Academy of Sciences, Washington, D.C. (1974).

Swift, D. W., R. W. Smith and S. I. Akasofu, "Imaging the Earth's magnetosphere", **Planet. Space Sci. 37**, 379, (1989).

Torr, D. G., M. R. Torr, M. Zukic, J. Spann and R. B. Johnson,"The ultraviolet imager (UVI) for ISTP", **Proc. SPIE Vol. 1745** , 61 (1992).

Torr, M. R., D. G. Torr, M. Zukic, J. F. Spann and R. B. Johnson, "An ultraviolet imager for the international solar terrestrial physics mission", **Space Sci. Rev.**, in press (1993).

Winter, H., and H. W. Ortjohann, "High transmission polarization analyzer for Lyman-α radiation", **Rev. Sci. Instrum. 58,** 359 (1987).

Wilson, M., J. Kim, M. Zukic, S. J ohn, D. G. Torr, A. Shapiro, P. Slane and J. Cobuzzi, "Optical constant determination for x-ray materials", to be presented at **SPIE** conference on X-Ray Technologies, San Diego, California, 11-16 July (1993).

Zukic, M., "Damped Least Squares Technique for the Design of Optical Multilayer Filters", M.S. Thesis, Imperial College, London (1984).

Zukic, M., "Optical Filters in the Vacuum Ultraviolet", PhD Dissertation, University of Alabama in Huntsville (1989).

Zukic, M., and K. Guenther, "Optical coatings with graded index layers for high power laser applications: design", **Proc. SPIE Vol. 895**, 270 (1988).

Zukic, M., and K. Guenther, "Design of nonpolarizing achromatic beamsplitters with dielectric multilayer coatings", **Opt. Eng. 28**, 165 (1989).

Zukic, M., and D. G. Torr, "High-reflective multilayers as narrowband VUV filters", **Proc. SPIE Vol. 1485**, 216 (1991).

Zukic, M., and D. G. Torr, "Multiple reflectors as narrowband and broadband VUV filters", **Appl. Opt. 31**, 1588 (1992a).

Zukic, M., and D. G. Torr, "VUV Thin Films", in **Topics in Applied Physics**, K. H. Guenther ed., Chapter VII, Spring-Verlag series on Thin Films, in press (1992b).

Zukic, M., D. G. Torr, J. F. Spann and M. R. Torr, "Vacuum ultraviolet thin films 1: Optical constants of BaF_2, CaF_2, LaF_3, MgF_2, Al_2O_3, HfO_2, and Si_2 thin films", **Appl. Opt. 29**, 4284 (1990a).

Zukic, M., D. G. Torr, J. F. Spann and M. R. Torr, "Vacuum ultraviolet thin films 2: Vacuum ultraviolet all-dielectric narrowband filters", **Appl. Opt. 29**, 4293 (1990b).

Zukic, M., D. G. Torr and M. R. Torr, "High throughput narrowband 83.4 nm self-filtering camera", **Proc. SPIE Vol. 1546**, 234 (1991).

Zukic, M., D. G. Torr and J. Kim, "Far ultraviolet filters for the ISTP imager", **Proc. SPIE Vol. 1745** , 99 (1992a).

Zukic, M., J. Kim and D. G. Torr, "Extreme ultraviolet filters for 58.4 and 83.4 nm", **Proc. SPIE Vol. 1744**, 178 (1992b).

Zukic, M., J. Kim, M. Wilson, J. Park and D. G. Torr, "Non-grazing high reflective narrowband multilayer x-ray coatings", to be presented at **SPIE** conference on X-Ray Technologies, San Diego, California, 11-16 July (1993a).

Zwiner, J. M., "Space station induced environment monitoring", **NASA Conference Publication 3021** (1988).

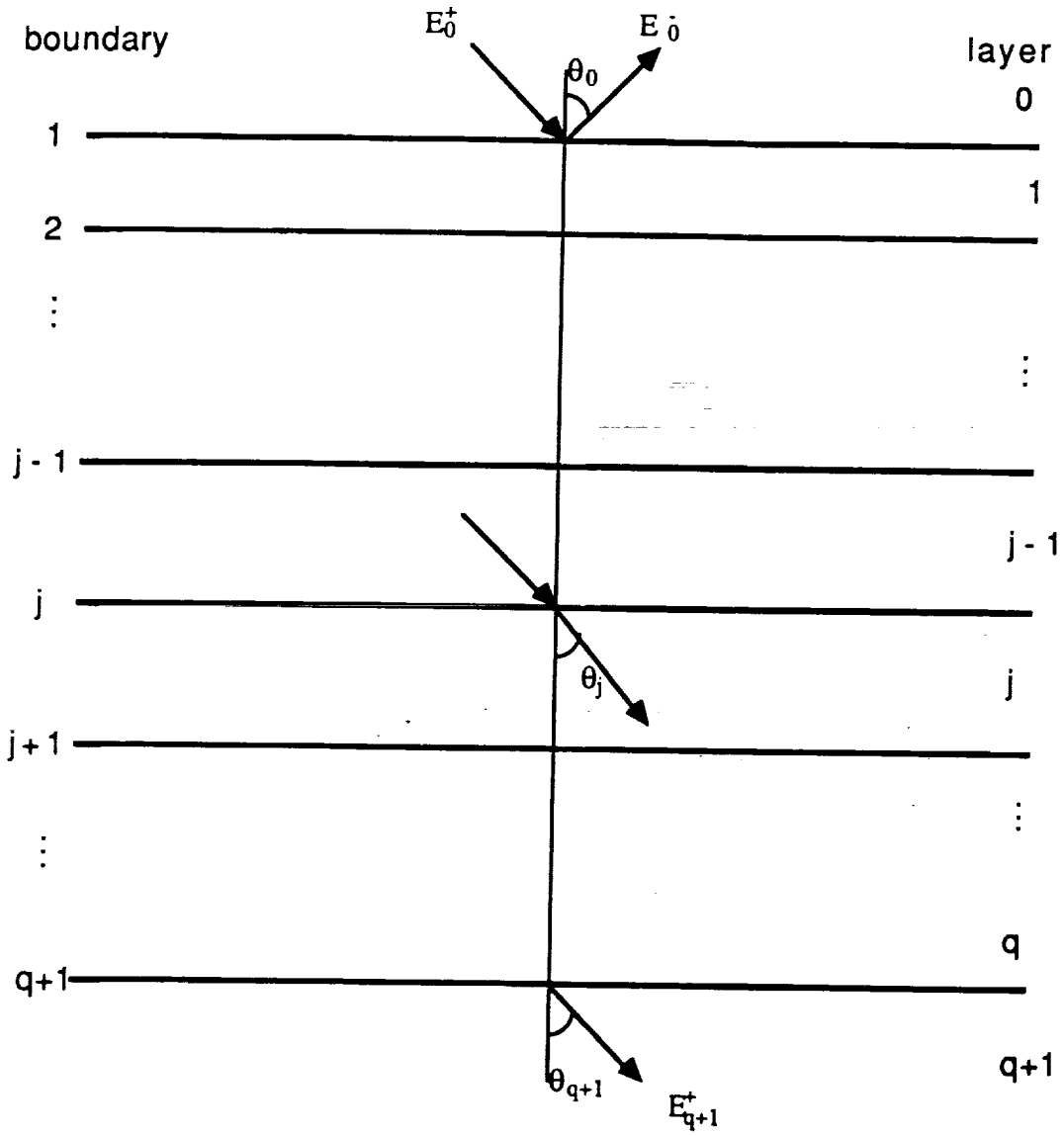

Figure 1. The optical configuration and notation of the multilayer thin film

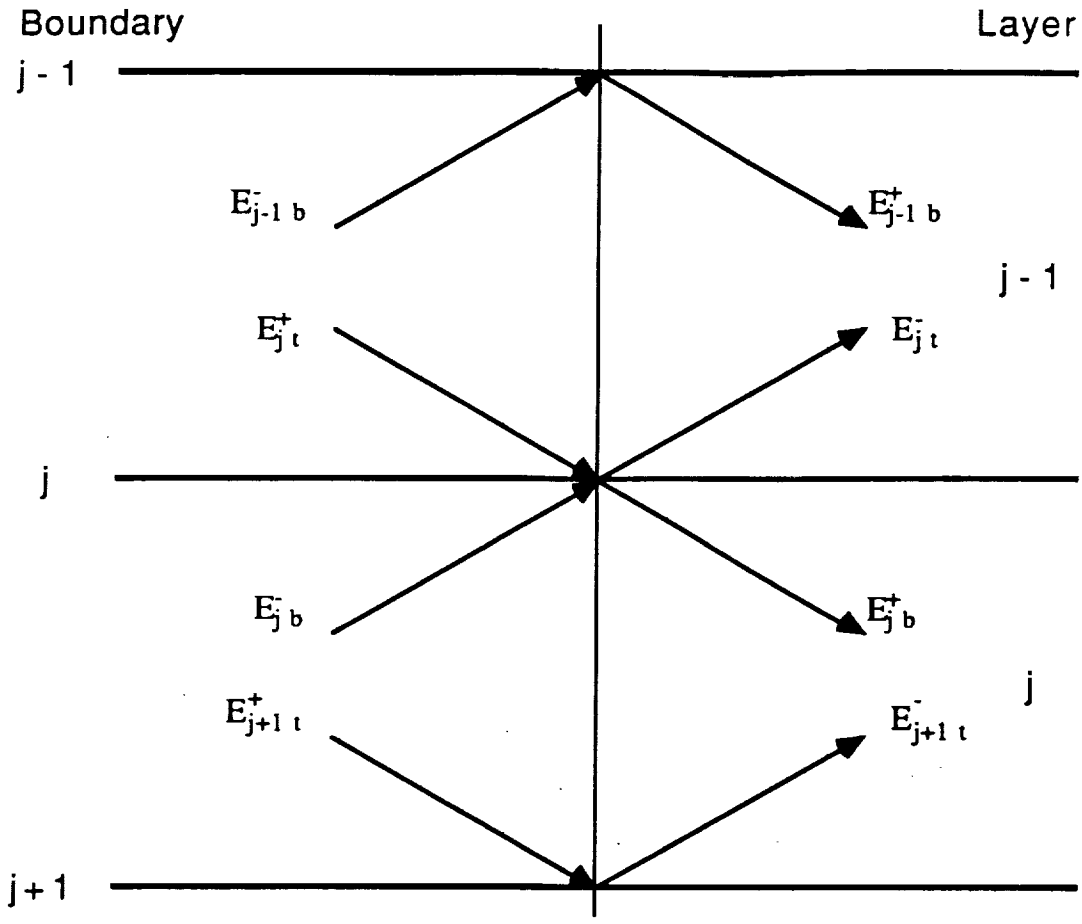

Figure 2. Electric fields at the j-th boundary.

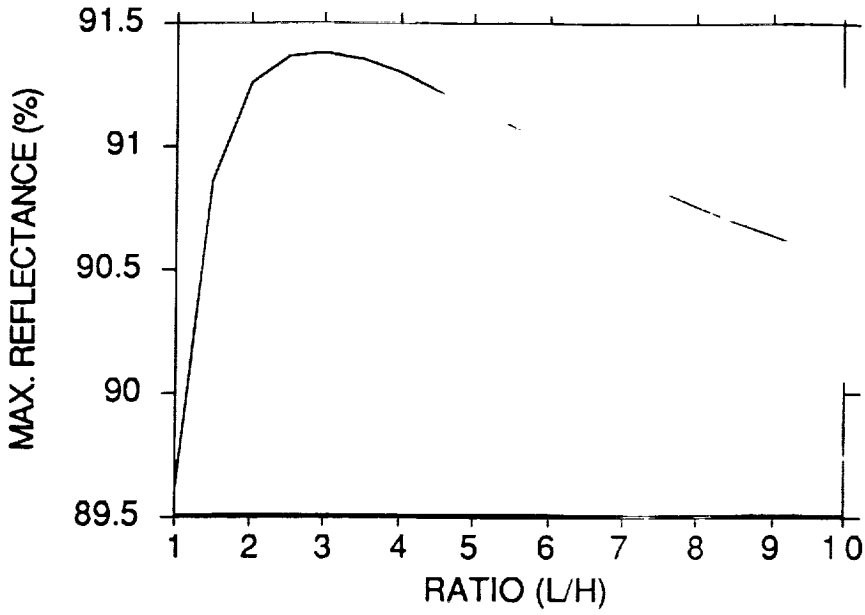

Figure 3. Change in the calculated reflectance of a Π-multilayer structure as the ratio(L/H) changes. The Koppelmann limit for this case is 89.6%.

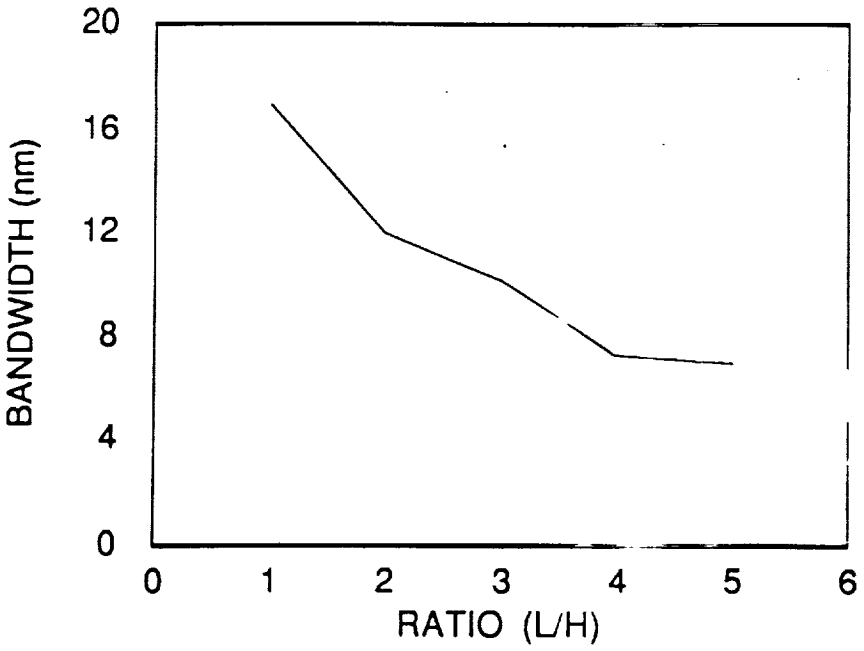

Figure 4. Full width at half of the reflectance maximum of the Π-stacks calculated for a 45° angle of incidence at 135.5 nm. H is for LaF_3, and L is for MgF_2.

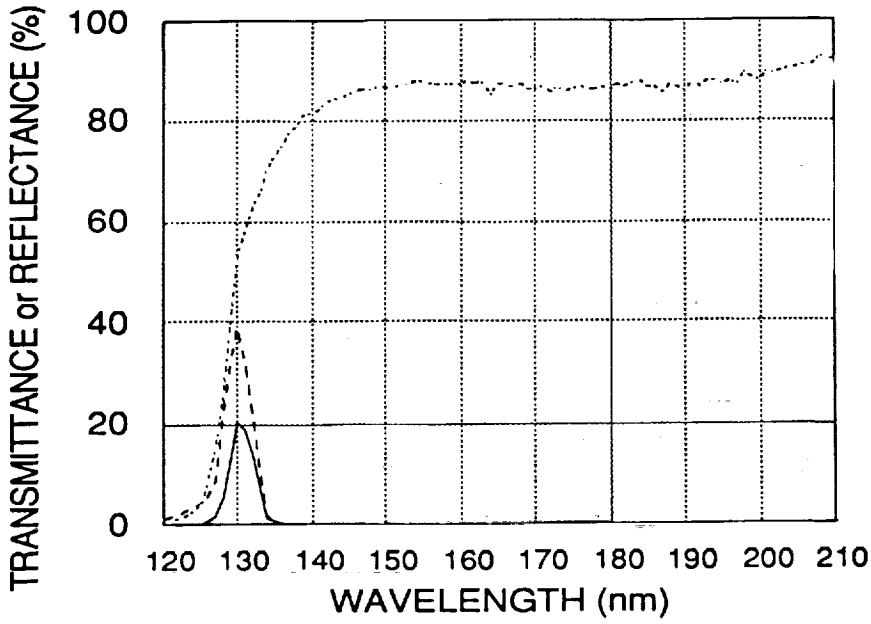

Figure 5. The measured net transmittance (solid line) through three narrowband reflection filters (dashed line) centered at 130.4 nm, and combined with the transmission filter (dotted line).

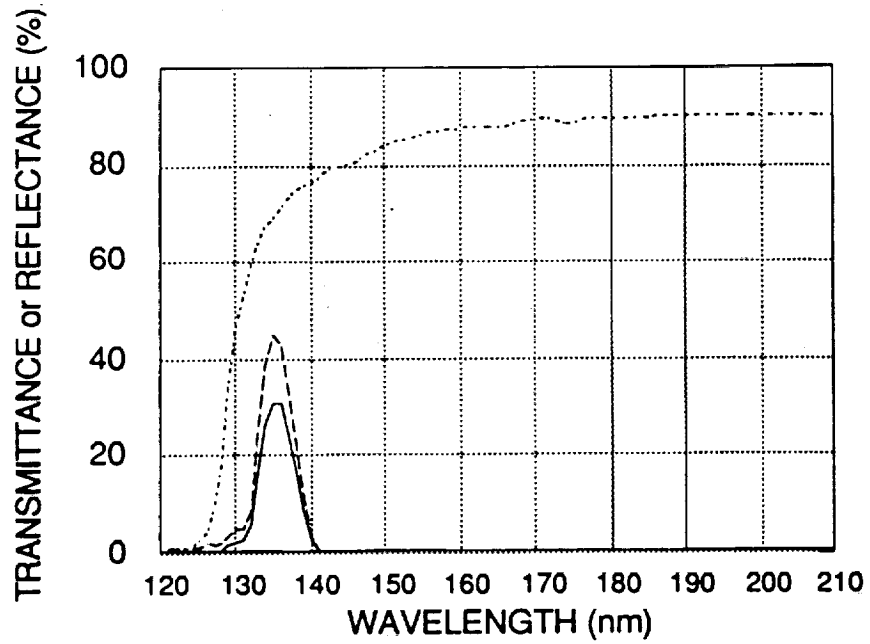

Figure 6. The measured net transmittance (solid line) through three narrowband reflection filters (dashed line) centered at 135 nm, and combined with the transmission filter (dotted line).

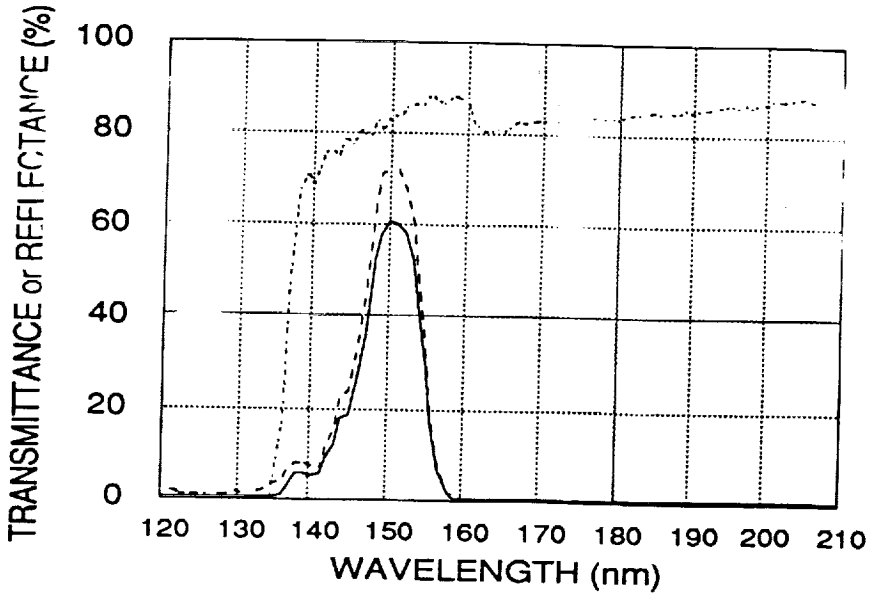

Figure 7. The measured net transmittance (solid line) through three broadband reflection filters (dashed line) centered at 150 nm, and combined with the transmission filter (dotted line).

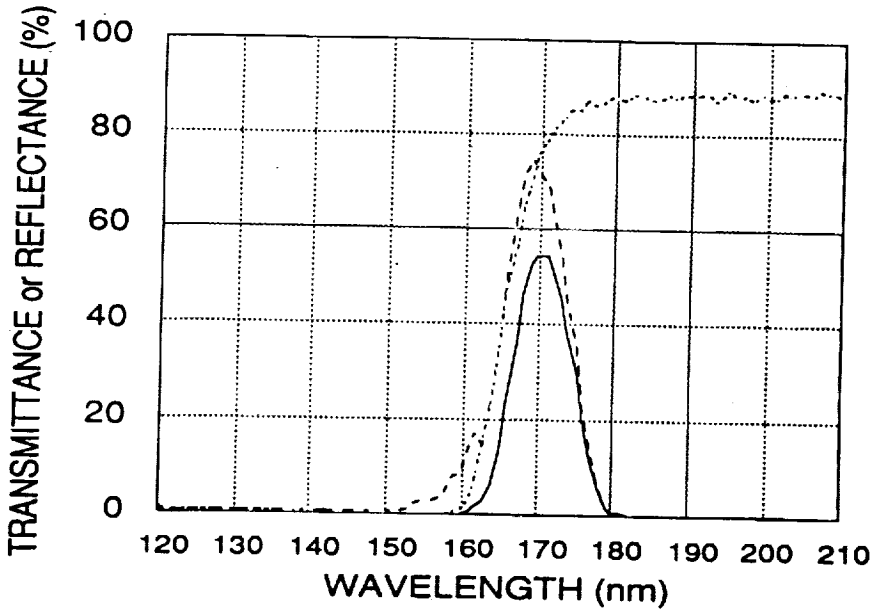

Figure 8. The measured net transmittance (solid line) through three broadband reflection filters (dashed line) centered at 170 nm, and combined with the transmission filter (dotted line).

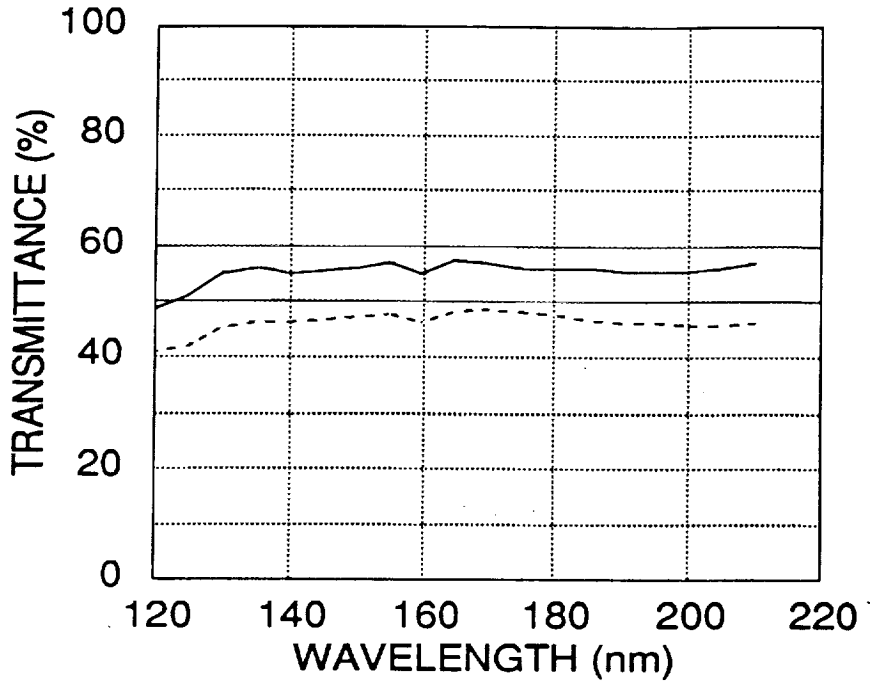

Figure 9. The measured transmittance of two FUV transparent conductive coatings. Solid line represents transmittance of a coating with 6500 Ω, and dashed line represents transmittance of a coating with 797 Ω resistance.

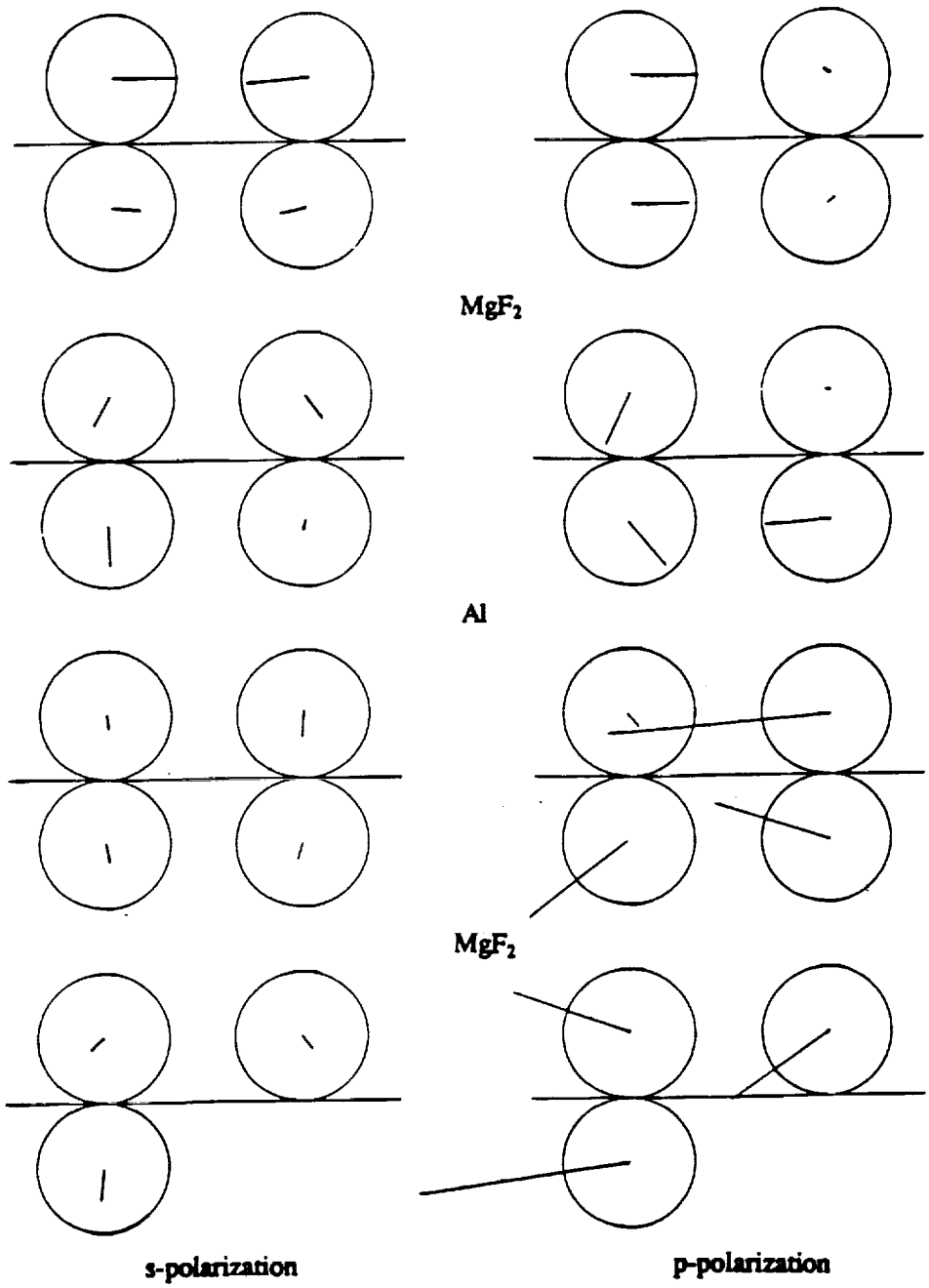

Figure 10. Incoming and outgoing electric fields at the top and bottom of each boundary for the 121.6 nm QWR case for the s- and p-polarization respectively. The left hand side is the incoming wave, and the right hand side is the outgoing wave for each polarization.

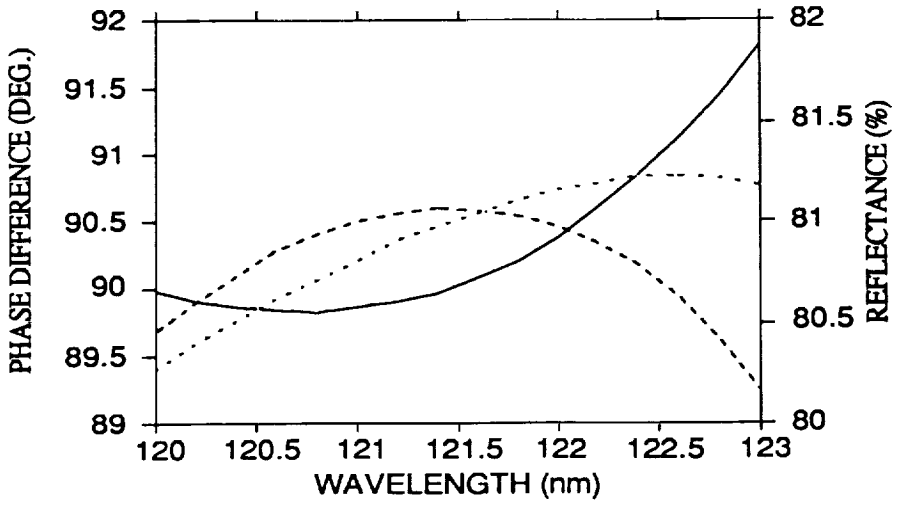

Figure 11. Calculated reflectances for s-polarization (dashed line) and p-polarization (dotted line), and the phase difference (solid line) between the two polarizations of a qurterwave retarder designed for the Lyman-α line at a 45° angle of incidence.

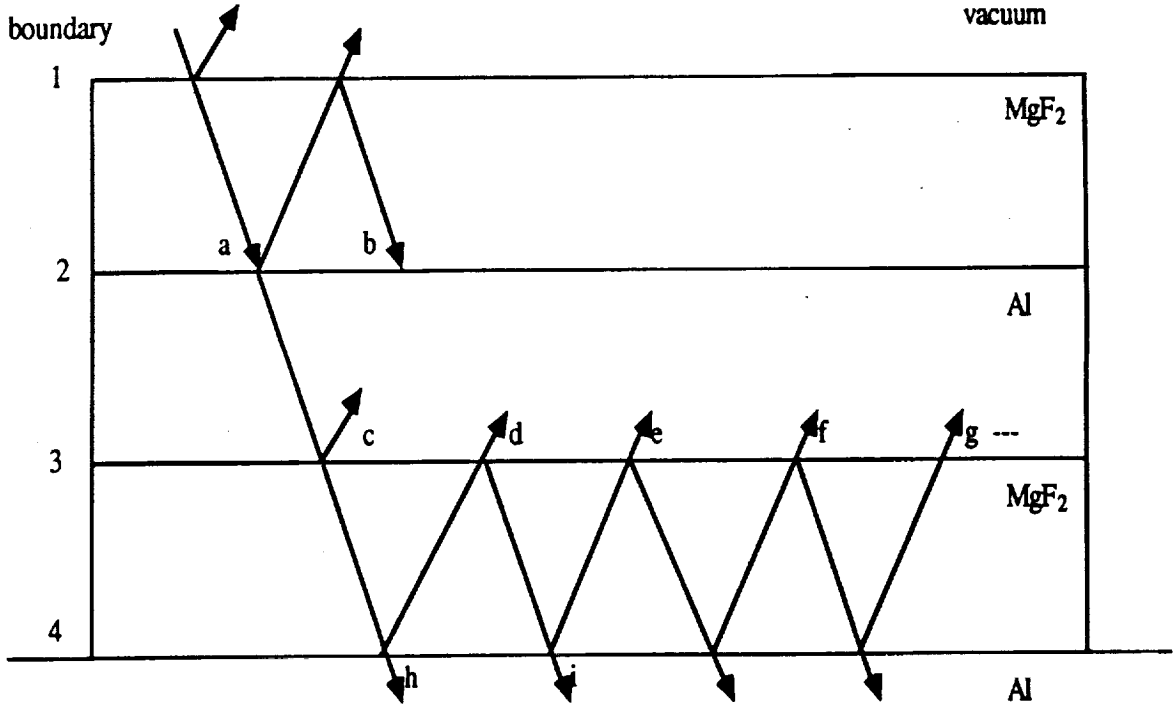

Figure 12. Important light waves for estimation of the thicknesses of the MgF_2 layers.

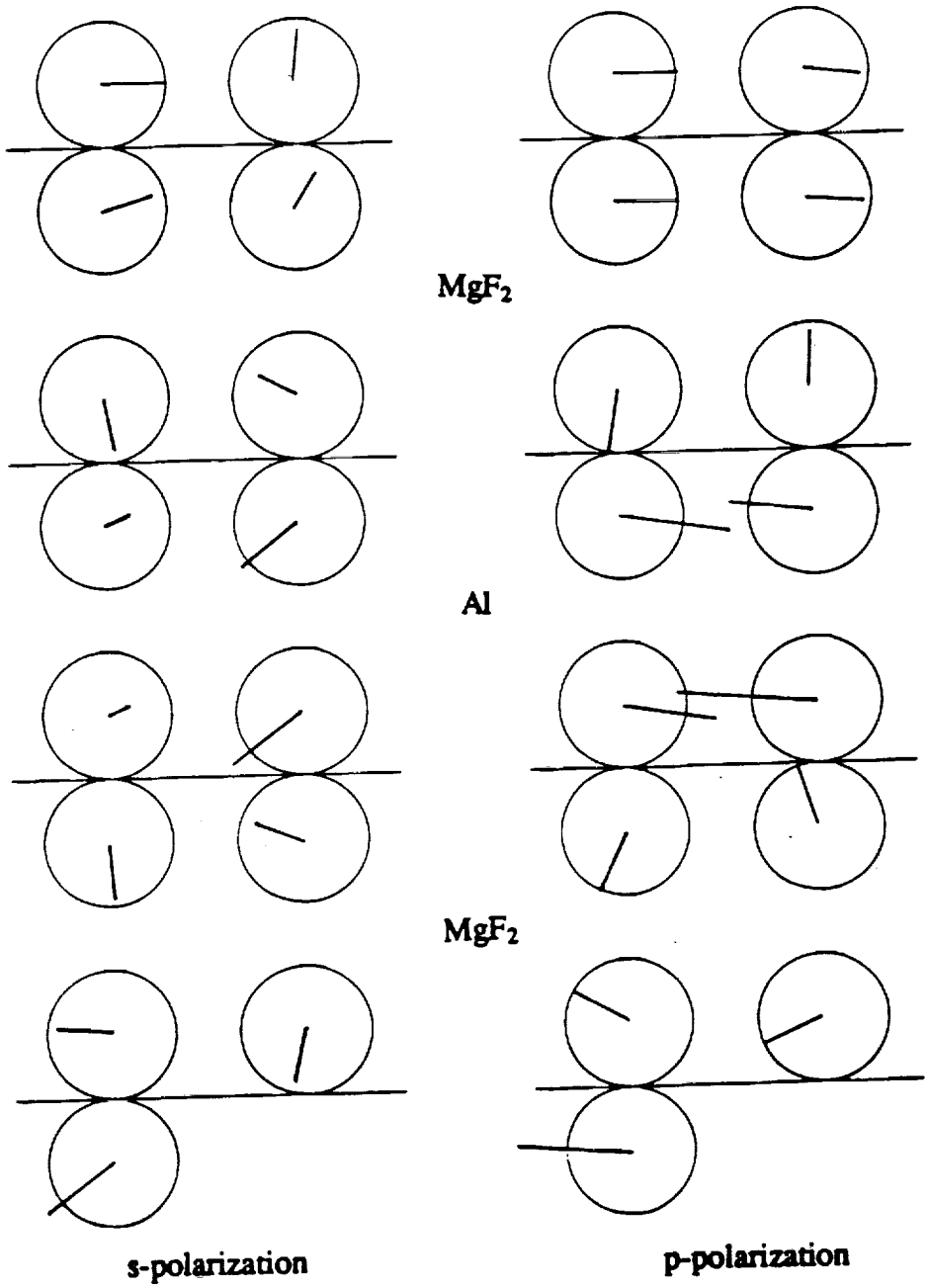

Figure 13. Incoming and outgoing electric fields at the top and bottom of each boundary for the 121.6 nm polarizer case for s- and p-polarization, respectively. The left hand side is the incoming wave and the right hand side is the outgoing wave for each polarization.

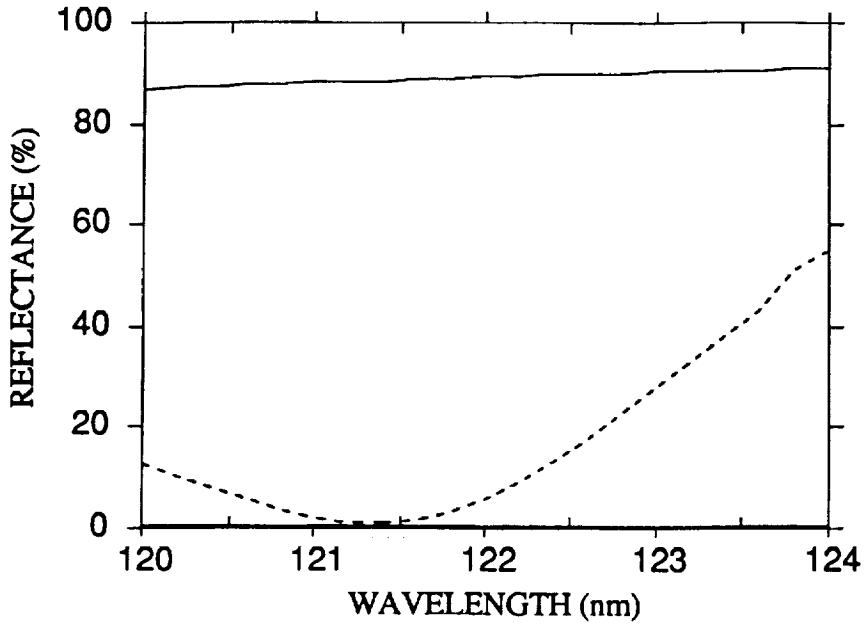

Figure 14. Calculated reflectances for s-polarization (solid line) and p-polarization (dashed line) of a polarizer designed for the Lyman-α line at a 45° angle of incidence

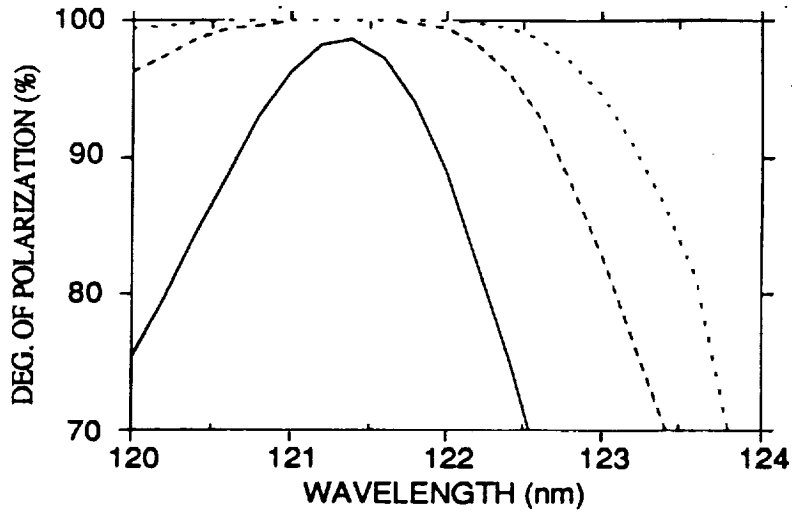

Figure 15. Calculated degrees of polarization for the single (solid line), double (dashed line) and triple (dotted line) reflection from the polarizer shown in Figure 5.

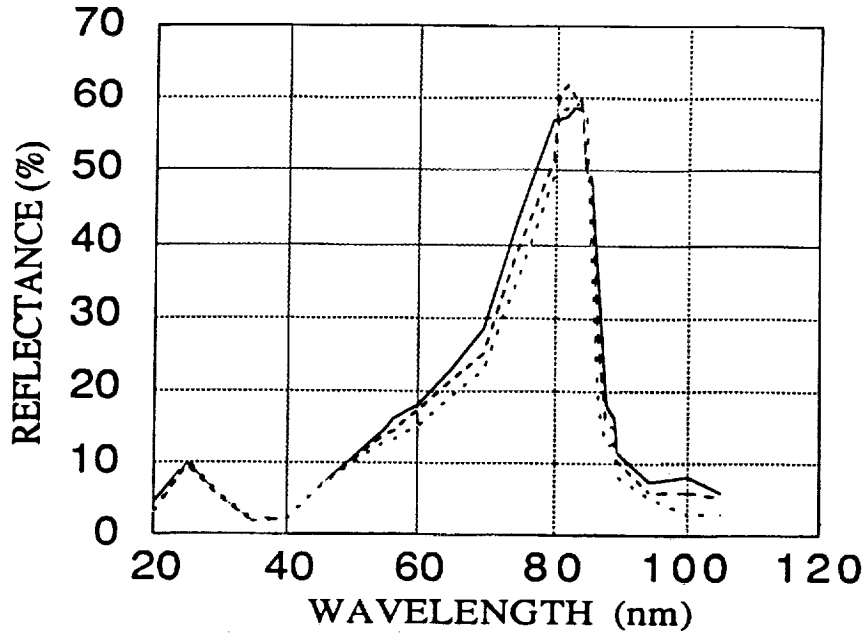

Figure 16. The calculated reflectance of Ge/MgF_2 stack for 10° (solid line), 30° (dashed line), and 50° angles of incidence (dotted lines).

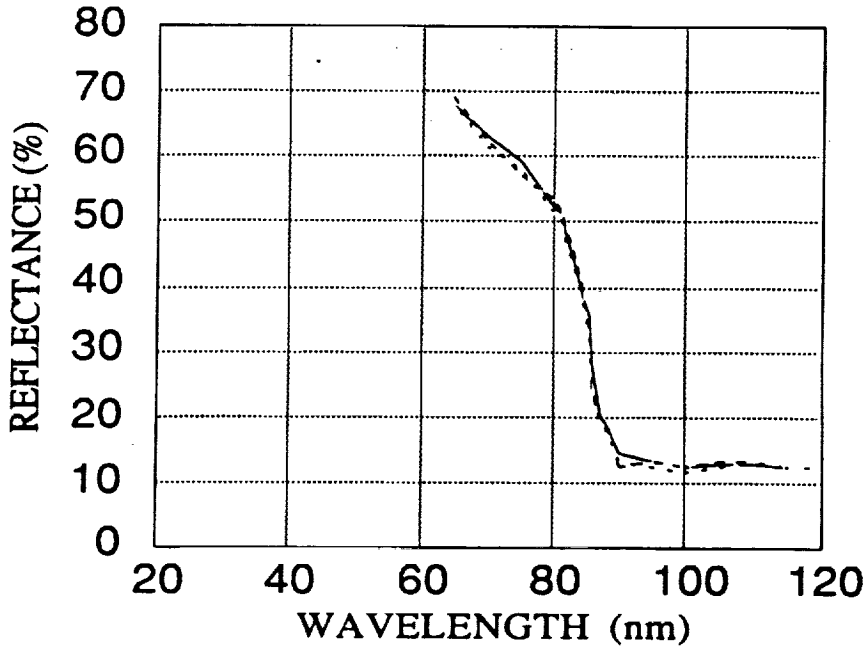

Figure 17. The measured reflectance of Ge/MgF_2 stack for 10° (solid line), 30° (dashed line), and 50° (dotted line) angles of incidence.

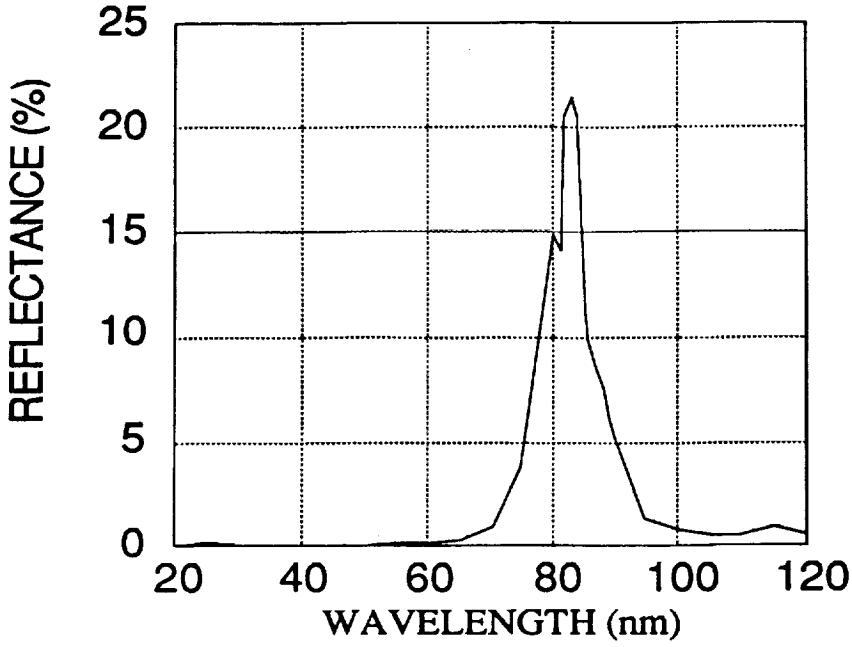

Figure 18. The calculated transmittance of the 83.4 nm self-filtering camera. The peak transmittance is greater than 20% with a bandwidth of 6.8 nm and an average out-of-band transmittance of less than 0.1%. The transmittance at 30.4 nm is 0.03%, at 58.4 nm and 121.6 nm the transmittance is 0.05% and 0.004%, respectively.

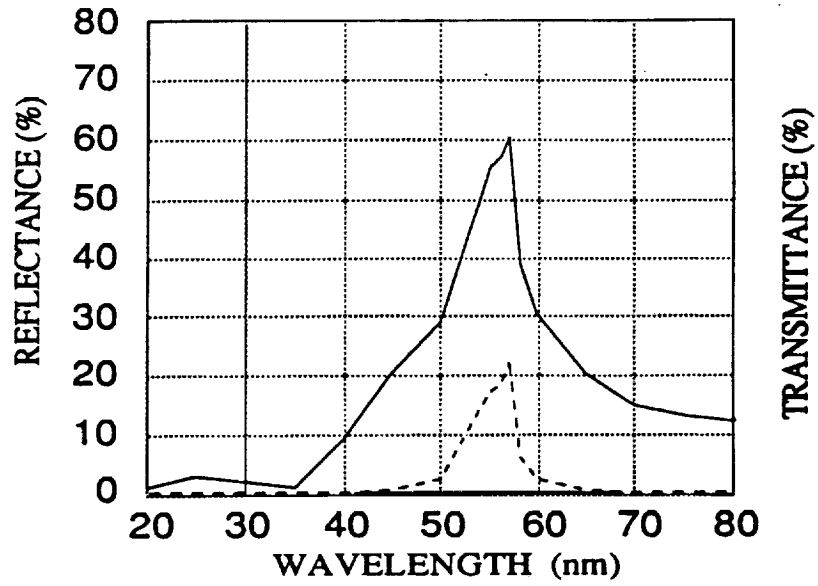

Figure 19. The calculated transmittance of a SiC/MgF_2 Π multilayer (solid line) The dashed line represents transmittance of a 58.4 nm self-filtering camera. The peak transmittance of the camera is greater than 20% with 8 nm bandwidth, and out-of-band rejection is better than 0.1% and .

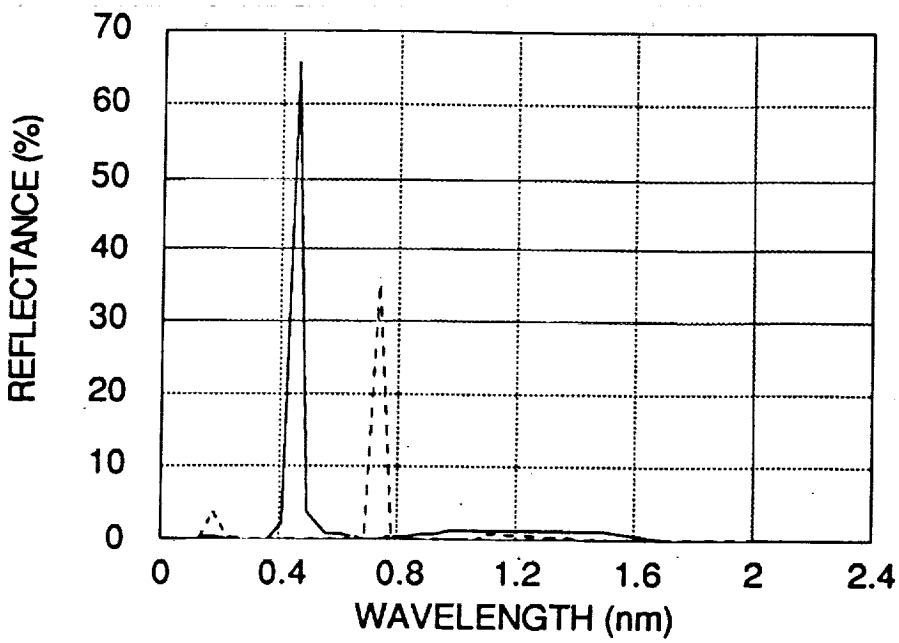

Figure 20. The calculated reflectance of a 99-layer stack. The solid line represents an 85° angle of incidence, and the dashed line is for 80° angle of incidence.

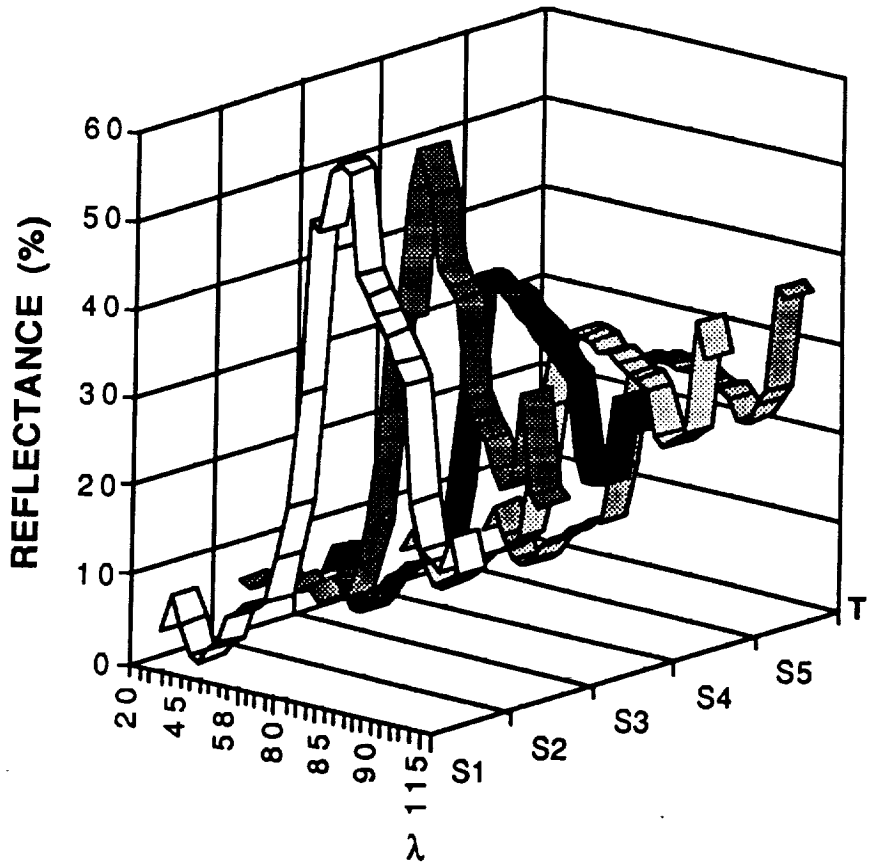

Figure 21. Computer modeling of the spectral deterioration of the EUV narrowband reflective coating (shown in Figs. 8 and 9). In the first step S1 it is assumed that the only degrading effect is erosion. The second step S2 starts at the point when Ge and MgF_2 are eroded away and the exposed film is Al. Since Al is highly corrosive material it is assumed that it will oxidize at a faster rate than erosion. Step S3: added surface contaminant, and steps S4 and S5 combine all pervious effects at the same rate.